

Tu E 14

Comparison of TTI and VTI 3D Inversion of CSEM Data

K.R. Hansen* (EMGS), M. Panzner (EMGS), D. Shantsev (EMGS), K. Mohn (MultiClient Geophysical)

Summary

Electrical anisotropy of steeply-dipping sedimentary rock formations can have a significant effect on marine CSEM data. We demonstrate how this TTI anisotropy can be taken into account in a 3D CSEM inversion, and compare VTI and TTI inversion results for a synthetic model and a CSEM field data set acquired over steeply-dipping geology. The results show that VTI inversion of CSEM data is inadequate in anisotropic, steeply-dipping geology, leading to spurious resistivity anomalies, whereas the TTI inversion produces geologically sound resistivity models with a better data fit.

Introduction

Electrical anisotropy of sedimentary rocks can be significant, in particular in shale formations (Ellis et al., 2010). The intrinsic anisotropy of such shale formations has been shown by Clavaud (2008) to be mainly due to compaction, and is therefore expected to be transversely isotropic. Controlled source electromagnetic (CSEM) data, acquired using a horizontal electric dipole, is sensitive to electrical anisotropy, since both vertical and horizontal electric currents are induced in the subsurface. It is therefore important to take anisotropy properly into account when imaging and interpreting such data (Mohamad et al., 2010).

Numerous publications have discussed the impact of vertical transversely isotropic (VTI) anisotropy on marine CSEM data, using both forward modeling (Lu and Xia, 2007) and inversion (Newman et al., 2010). This VTI assumption is suitable for sedimentary rock formations with approximately horizontal bedding. For dipping formations, however, the additional effect of the tilted transversely isotropic (TTI) formation can have a significant impact on marine CSEM data, as shown by Davydycheva and Frenkel (2013). In this paper, we show how TTI anisotropy can be included in a 3D inversion of marine CSEM data and compare VTI and TTI imaging results for a synthetic model and a CSEM field data set acquired over steeply dipping geology.

Method

TTI forward modeling of CSEM data

The electric and magnetic fields comprising CSEM data are governed by Maxwell's equations in the quasi-static limit

$$\nabla \times \mathbf{E} = -\mu_0 \frac{\partial \mathbf{H}}{\partial t}, \quad \nabla \times \mathbf{H} = \Sigma \mathbf{E} + \mathbf{J}, \quad (1)$$

where \mathbf{E} and \mathbf{H} are the electric and magnetic field vectors, respectively, μ_0 is the vacuum magnetic permeability, \mathbf{J} is the source current density and Σ is the conductivity tensor of the medium. In the VTI approximation, the conductivity tensor is diagonal in a cartesian coordinate system aligned with the vertical and horizontal directions, with the two diagonal components corresponding to the horizontal directions having the same value σ_h , and the diagonal component corresponding to the vertical direction denoted σ_v . If the bedding of the subsurface is not horizontal, the conductivity tensor is no longer diagonal, but is instead given by

$$\Sigma = \mathbf{R}^T \begin{pmatrix} \sigma_p & & \\ & \sigma_p & \\ & & \sigma_n \end{pmatrix} \mathbf{R} \quad (2)$$

where σ_p and σ_n are the bed-parallel and bed-normal components of the conductivity tensor Σ in a coordinate system aligned with the formation bedding. The rotation matrix \mathbf{R} is given by

$$\mathbf{R} = \begin{pmatrix} \cos \alpha \cos \beta & \sin \alpha \cos \beta & -\sin \beta \\ -\sin \alpha & \cos \alpha & 0 \\ \cos \alpha \sin \beta & \sin \alpha \sin \beta & \cos \beta \end{pmatrix}, \quad (3)$$

where the two Euler angles α and β measure the azimuth and dip of the formation, respectively.

We numerically solve Maxwell's equations by a finite-difference time-domain method, using a Lebedev grid to handle the TTI anisotropic medium. To obtain an efficient algorithm, the problem is first transformed from the actual quasi-static domain, in which conduction currents dominate, to a fictitious wave domain where displacement currents dominate (Maaø, 2007).

3D TTI inversion of CSEM data

We formulate the CSEM inverse problem as a nonlinear least squares problem, with a cost function given by

$$E(\mathbf{m}) = E_d(\mathbf{m}) + \lambda E_r(\mathbf{m}), \quad (4)$$

where \mathbf{m} is a vector of model parameters ($\ln \sigma_n, \ln \sigma_p, \alpha, \beta$) for each model cell, E_d is the data misfit cost function, E_r is the regularization cost function and λ is a trade-off parameter between data misfit and regularization. The data misfit is the least squares cost function

$$E_d(\mathbf{m}) = \frac{1}{N_d} \left(\mathbf{d}^{obs} - \mathbf{d}^{syn}(\mathbf{m}) \right)^\dagger \mathbf{W}_d^T \mathbf{W}_d \left(\mathbf{d}^{obs} - \mathbf{d}^{syn}(\mathbf{m}) \right), \quad (5)$$

where N_d is the number of data points, \mathbf{d}^{obs} is a vector of frequency-domain CSEM data and \mathbf{d}^{syn} the corresponding vector of synthetic data for the model given by \mathbf{m} . The diagonal matrix \mathbf{W}_d is a data weighting matrix, whose diagonal elements are the inverse standard deviations for the observed data. The data standard deviations have a contribution from the ambient noise, which is independent of the CSEM signal, and a contribution from uncertainty in the acquisition parameters, which is approximately proportional to the CSEM signal amplitude (Mittet and Morten, 2012).

The regularization cost function E_r is a discretized version of the functional

$$\varepsilon_r(m) = \frac{1}{V} \int |\mathbf{A} \nabla' (m - m^{ap})|^2 dV = \frac{1}{V} \int |\mathbf{A} \mathbf{R} \nabla (m - m^{ap})|^2 dV, \quad (6)$$

where V is the volume of the model domain, $\nabla' m = \mathbf{R} \nabla m$ is the gradient of the model m with respect to the local bedding-aligned coordinate system and m^{ap} is an a priori model, which is typically chosen to be the initial model in the inversion. Using the local bedding-aligned coordinate system rather than the ordinary model coordinate system is more appropriate in steeply-dipping formations, since the smoothing effect of the regularization will tend to follow the dipping formation better. The 3×3 diagonal matrix \mathbf{A} contains weights for each of the three spatial derivatives of m . The diagonal elements are

$$A_{11} = A_{22} = a_T, \quad A_{33} = a_N \quad (7)$$

where a_T is the weight for the transverse (x', y') spatial derivatives and a_N is the weight for the normal (z') spatial derivative. For sedimentary rock formations, we choose $a_T \gg a_N$, since we expect greater variation of conductivity in the direction normal to the bedding compared to directions parallel to the bedding.

The total cost function given in equation (4) is minimized using the L-BFGS-B algorithm by Zhu et al. (1997). This algorithm requires only the gradient of the cost function, which is calculated using the adjoint state method (Støren et al., 2008).

Results

Synthetic anticline model

We first apply our inversion algorithm to a synthetic CSEM data set. The synthetic model, shown in Figure 1, is a simple 2D TTI anisotropic anticline model with anisotropy ratio $\sigma_p/\sigma_n \approx 2$ and with a small resistive anomaly of 50 Ωm at the crest of the structure. The synthetic CSEM survey consists of 3 lines of receivers with a line separation of 1 km, each with 19 ocean bottom receivers with 1 km separation, recording the horizontal electric field components. The source is a horizontal electric dipole towed along the 3 receiver lines and with 2 additional azimuth lines on each side of the receiver grid for a total of 7 towlines. The source separation along each line is 100 m. The data consisted of the horizontal electric field components at 3 frequencies of 0.25 Hz, 0.5 Hz and 1 Hz with source-receiver offset up to 10 km. The synthetic data was contaminated by 1% Gaussian multiplicative noise and additive noise with a standard deviation of 10^{-16} V/Am².

The result of our TTI inversion compared to a VTI inversion, in which the azimuth and dip angles are set to zero, is shown in Figure 2. The TTI inversion produces a clear anomaly at the approximate position of the reservoir. The VTI inversion produces a weaker anomaly at the reservoir location, and in addition produces resistivity artifacts on the flanks of the anticline, where the dip is highest. The TTI inversion converged to an RMS data misfit of 0.82, while the VTI inversion converged to an RMS data misfit of 0.9. Both inversions thus produced a good fit to the data.

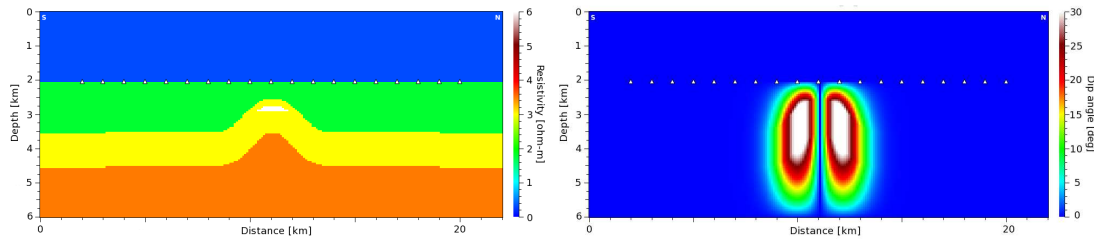


Figure 1 Normal resistivity component (left) and dip angle (right) of the synthetic model. The target resistivity is 50 ohm-m, and the yellow triangles indicate receiver positions along the center towline.

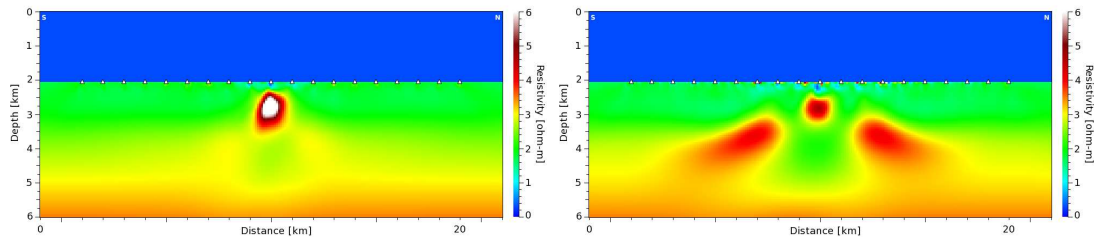


Figure 2 Normal/vertical resistivity component for a TTI (left) and VTI (right) inversion of the synthetic data set from the model shown in Figure 1.

Real data example

We next apply our inversion algorithm to a field data set from the Gulf of Mexico. The survey consisted of 184 receivers, with a spacing of 1.5 km, and 24 towlines, and we included the horizontal electric field components at frequencies of 0.15625 Hz, 0.46875 Hz and 0.78125 Hz for source-receiver offsets up to 13 km in the inversion. The initial model, shown in Figure 3, was constructed from an increasing resistivity gradient that approximately follows the main features of the stratigraphy. For the TTI inversion, the initial values for the dip and azimuth angles were estimated by interpolating the dip and azimuth of the main horizons identified from seismic data, and varied with dip values up to 30 - 50 degrees on the flanks of the anticline. The inversion was free to change the angles, but only minor changes of a few degrees were produced by the inversion. The final inverted conductivity models are also shown in Figure 3 for the VTI and TTI inversion superimposed on PSDM seismic. There are clear differences between the VTI and TTI results, with the TTI inversion result showing an increased resistivity in a layer following the main stratigraphic trends. The VTI inversion result shows resistive anomalies that do not seem to match the stratigraphy and are thus most likely artifacts caused by the VTI anisotropy constraint. Furthermore, the TTI inversion converged to an RMS data misfit of 1.26, while the VTI inversion converged to an RMS data misfit of 2.13. The TTI inversion result thus has a significantly better data fit than the VTI inversion result in addition to being a more geologically meaningful model.

Conclusions

We have implemented a 3D inversion for CSEM data that takes TTI anisotropy fully into account. By comparing VTI and TTI inversion of a TTI synthetic model, we showed that the image produced by the VTI inversion contains spurious artifacts due to the inadequate description of the anisotropy. Applying our algorithm to a 3D CSEM data set acquired in the Gulf of Mexico over steeply-dipping geology, we found that the TTI inversion converged to a better data fit and produced a more geologically meaningful conductivity model compared to a VTI inversion.

Acknowledgements

We would like to thank MultiClient Geophysical for permission to use the seismic data covering the Gulf of Mexico CSEM survey, Honglin Yuan for assistance with the real data inversions and EMGS for

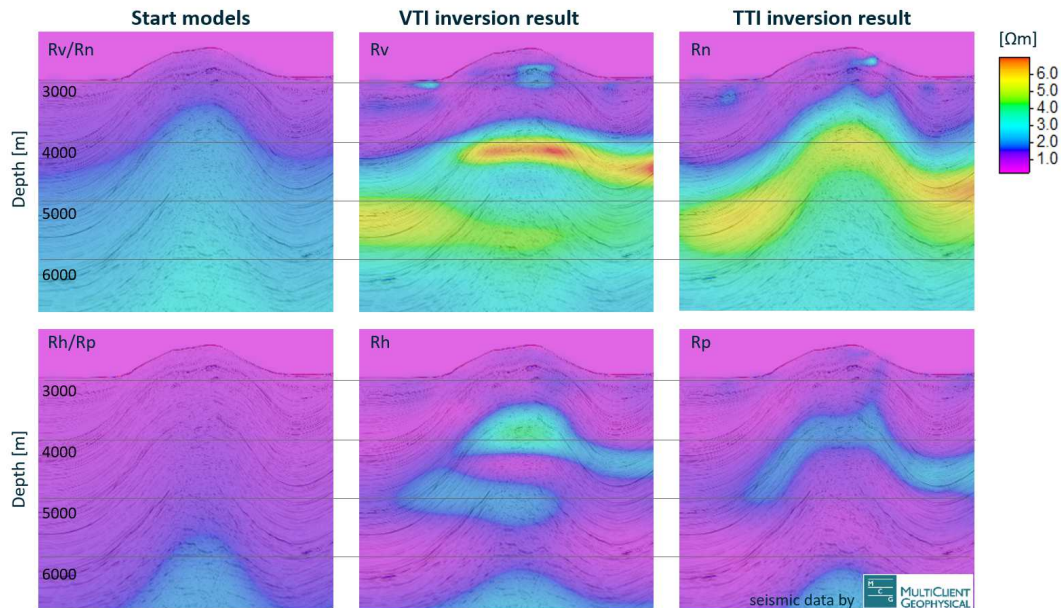


Figure 3 Resistivity components of the start model (left), VTI inversion result (middle) and TTI inversion result (right). Top row shows the normal resistivity component, bottom row shows the parallel resistivity component.

permission to publish the results.

References

- Clavaud, J.B. [2008] Intrinsic Electrical Anisotropy of Shale: The Effect of Compaction. *Petrophysics*, **49**(3), 243–260.
- Davydycheva, S. and Frenkel, M.A. [2013] The impact of 3D tilted resistivity anisotropy on marine CSEM measurements. *The Leading Edge*, **32**(11), 1374–1381.
- Ellis, M., Sinha, M. and Parr, R. [2010] Role of fine-scale layering and grain alignment in the electrical anisotropy of marine sediments. *First Break*, **28**(9), 49–57.
- Lu, X. and Xia, C. [2007] Understanding anisotropy in marine CSEM data. In: *SEG Technical Program Expanded Abstracts*. SEG, 633–637.
- Maaø, F.A. [2007] Fast finite-difference time-domain modeling for marine-subsurface electromagnetic problems. *Geophysics*, **72**(2), A19–A23.
- Mittet, R. and Morten, J.P. [2012] Detection and imaging sensitivity of the marine CSEM method. *Geophysics*, **77**(6), E411–E425.
- Mohamad, S.A., Lorenz, L., Hoong, L.T., Wei, T.K., Chandola, S.K., Saadah, N. and Nazihah, F. [2010] A practical example why anisotropy matters. A CSEM case study from South East Asia. In: *SEG Technical Program Expanded Abstracts*. SEG, 696–700.
- Newman, G.A., Commer, M. and Carazzone, J.J. [2010] Imaging CSEM data in the presence of electrical anisotropy. *Geophysics*, **75**(2), F51–F61.
- Støren, T., Zach, J.J. and Maaø, F.A. [2008] Gradient calculations for 3D inversion of CSEM data using a fast finite-difference time-domain modelling code. In: *70th EAGE Conference & Exhibition*. EAGE, P194.
- Zhu, C., Byrd, R.H., Lu, P. and Nocedal, J. [1997] Algorithm 778: L-BFGS-B: Fortran subroutines for large-scale bound-constrained optimization. *ACM Transactions on Mathematical Software (TOMS)*, **23**(4), 550–560.